Optical Engineering

SPIEDigitalLibrary.org/oe

Analysis of laser speckle severity, granularity, and anisotropy using the power spectral density in polar-coordinate representation

Desmond C. Ong
Sanjeev Solanki
Xinan Liang
Xuewu Xu

Analysis of laser speckle severity, granularity, and anisotropy using the power spectral density in polar-coordinate representation

Desmond C. Ong
Sanjeev Solanki
Xinan Liang
Xuewu Xu
Data Storage Institute
A*STAR (Agency for Science, Technology and Research)
Singapore 117608, Singapore
E-mail: co92@cornell.edu

Abstract. The conventional speckle contrast measures only speckle severity, and is unable to characterize granularity and anisotropy in displayed images, which are easily picked up by human observers. Here, we propose a comprehensive method based on the power spectral density which allows the simultaneous measurement of three components of laser speckle-severity, granularity and anisotropy—as a superior way to evaluate both speckle and speckle reduction techniques. [DOI: 10.1117/1.OE.51.5.054301]

Subject terms: speckle analysis; power spectral density; laser display; holographic display.

Paper 120261 received Feb. 24, 2012; revised manuscript received Mar. 28, 2012; accepted for publication Apr. 2, 2012; published online May 4, 2012.

1 Introduction

Speckle arises from coherent interference, such as of laser light that is reflected off a rough surface, and manifests itself as random granular noise.[1,2] Such speckle patterns can be useful, such as in speckle metrology,[3] dynamic speckle interferometry,[4] and speckle profilometry,[5] but in many other applications, speckle is unwanted and results in loss of information, such as in ultrasound imaging.[6] In particular, speckle is detrimental to laser-based imaging systems, such as laser-based televisions (TVs) and projectors,[7–9] and holographic display systems,[10] as it introduces aesthetically displeasing noise. It is thus essential to have a metric which is able to accurately characterize speckle noise and speckle reduction techniques for laser display purposes.

The most commonly used metric to evaluate speckle severity is the speckle contrast ($C = \sigma/\langle I \rangle$), defined as the standard deviation of intensity normalized by the mean intensity.[1,2] This is sufficient in applications where the information in a signal or image is contained only in the individual intensity values and not in correlations between neighboring pixels. In a displayed image, however, local correlations in intensities are essential to define edges, boundaries and features, and the speckle contrast, being a pixel-centric method, is unable to pick up speckle features related to such local correlations. Two examples of such features are granularity and anisotropy in the speckle pattern. In particular, anisotropy can be a pertinent problem—many speckle reduction methods require some form of "movement" in order to break spatial coherence and reduce speckle. These methods can involve both hardware, such as rotating diffusers,[11] or software, such as cyclically shifting the hologram.[12] If there was any anisotropy in the application of these methods, the spatial coherence and consequently speckle would be retained along certain directions, resulting in an anisotropic distribution of speckle. An example of how speckle degrades the aesthetic quality of displayed images is shown in Fig. 1(a) and 1(b), with examples of isotropic and anisotropic speckle reduction in Fig. 1(c) and 1(d).

The speckle contrast considers only the standard deviation of the pixel intensities, without considering correlations between pixels. One has to turn to correlation-based statistics to comprehensively characterize speckle. Such correlation analyses have naturally been used in some of the above-mentioned applications such as metrology,[3] and have recently been studied in imaging,[13] but not in an applicable way to characterize speckle reduction. In this paper, we adapt a formulation based on the power spectral density, or PSD, first studied in speckle by Goldfischer,[14] who related it to the autocorrelation function. We draw on the physical significance of the PSD as representing the power due to the different frequencies of intensity variation, and use the PSD in polar coordinates to find the angular distribution of power. A similar re-formulation of the PSD has recently been used for an entirely different purpose in surface morphology characterization.[15] The method described in this paper allows characterization of the speckle severity (what the speckle contrast measures), granularity (speckle grain size), and anisotropy. It provides a comprehensive characterization of speckled images, and can be used to evaluate current and future speckle reduction technologies. In the next few sections, we define the three characteristics of speckle, describe our method, and demonstrate its validity using experimentally captured images, before discussing the implications and ideas for future research.

2 Definition of Speckle Severity, Granularity, and Anisotropy

Refer to Fig. 2 for an illustration of the terms speckle severity, granularity and anisotropy. First, speckle severity refers to the magnitude of the speckle, that is, the total amount of variation in the image. The speckle contrast captures this variation precisely, by considering the standard deviation of the intensity values. Fig. 2(a) shows a one-dimensional line-scan through an ideal image, which has no variation due to speckle. In Fig. 2(b), we show an example of high

0091-3286/2012/$25.00

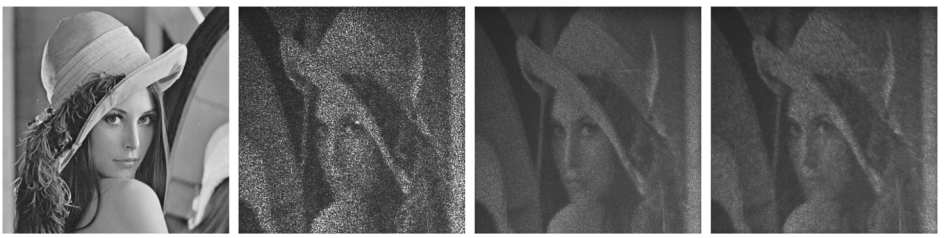

Fig. 1 Degradation of aesthetic quality by speckle. The images were captured using a holographic display system, described in the text. They are mirrored about the vertical axis due to the display optics: (a) original input image, (b) speckled reconstruction, (c) with isotropic speckle reduction applied, (d) with anisotropic speckle reduction applied. The speckle contrast, estimated from Lena's hat, is (b) 0.584, (c) 0.178, and (d) 0.180—it is unable to pick out the aesthetic difference between (c) and (d).

speckle severity, while in Fig. 2(c), we show a corresponding example of low speckle severity.

Second, speckle granularity refers simply to the distribution of speckle at different grain sizes. Grain size is independent of severity, and can be seen by comparing Fig. 2(c) which has a small grain size, and Fig. 2(d) which has the same severity and a larger grain size. Characterizing granularity is important because some speckle reduction methods may be constrained by certain length-scales, for example, the grain size on a random diffuser. This might have an effect on the grain structure of the speckle pattern after applying speckle reduction such as retaining speckle above a certain minimum size.

Third, speckle anisotropy refers to the inhomogeneous distribution of speckle with respect to direction. Anisotropic speckle patterns could have speckle that is longer in one direction as compared to another, or speckle distributions that favor a certain direction over another, or both. Consider the two images in Fig. 2(e) and 2(f), which have the same number of speckles and of the same size distributed evenly throughout the images. Figure 2(e) has a relatively random and isotropic distribution of speckle, while Fig. 2(f) has a distribution of speckle that favors the 45 degree line along the top-right to bottom-left direction. As mentioned in the introduction, application of an anisotropic speckle reduction method (e.g., vibration only in one direction) would destroy spatial coherence in one direction and retain spatial coherence in another direction, resulting in an anisotropic distribution. Not all speckle reduction methods require movement to break spatial coherence, such as polarization multiplexing and wavelength multiplexing; however for the methods that do, this is an important consideration.

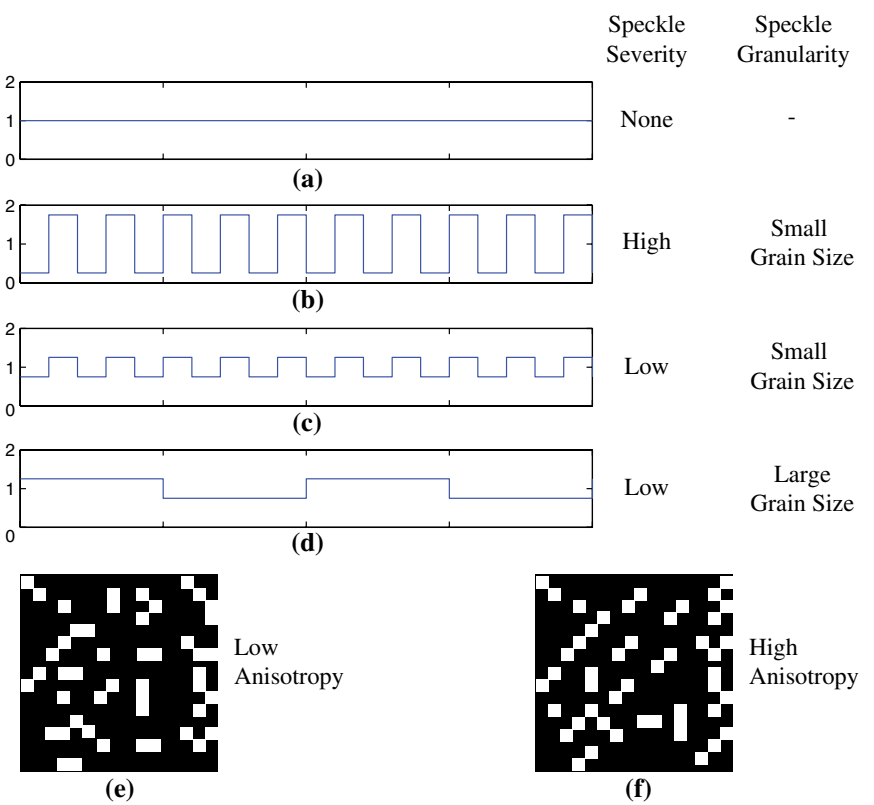

Fig. 2 Illustration of the terms speckle severity, speckle granularity, and anisotropy. (a) 1-D line-scan of an ideal image with no intensity variation, and hence no speckle. (b) High speckle severity with small grain size. (c) Low speckle severity with small grain size. (d) Low speckle severity with large grain size. (e) Image with low anisotropy. (f) Image with high anisotropy.

3 Description of the Speckle Analysis Method Using the Power Spectral Density

For a given speckled image, we seek to quantify the power contained in various spatial frequencies, and hence we borrow and adapt the formulation of the Power Spectral Density (PSD). There are two formulations of the PSD, either via periodogram or correlogram methods.[16] The former relates the PSD to the expectation of the squared Fourier Transform of the signal, while the latter (via the Wiener-Khinchin theorem) relates the PSD to the Fourier Transform of the autocorrelation function of the signal. The equivalency of the two can be shown via various methods, such as by brute force expansion or by the convolution theorem, and has been shown in many texts.[17,18] For our purposes, we consider the former, periodogram method for ease of computation.

Consider a two dimensional (2D) speckled image $A(x,y)$ of size $(2M+1,\ 2N+1)$. The 2D PSD is given by the squared modulus of the 2D Fourier Transform (FT):

$$\mathrm{PSD}_C(f_x,f_y)=\left|\sum_{\Delta x=-M}^{M}\sum_{\Delta y=-N}^{N}\left\{A(x,y)\times\exp\left[-i2\pi\left(\frac{f_x x}{2M+1}+\frac{f_y y}{2N+1}\right)\right]\right\}\right|^2, \quad (1)$$

where the PSD is not restricted to only positive frequencies. The subscript C denotes the fact that it is defined in Cartesian coordinates. $\mathrm{PSD}_C(f_x,f_y)$ yields the power contribution within the image $A(x,y)$ due to variations of spatial frequencies (f_x,f_y) along the x, y axes. The PSD can be normalized such that the zero-frequency term $\mathrm{PSD}_C(0,0)$, representing the square of the total brightness in the image, is equal to unity.

In order to study the angular distribution of speckle, we consider a simple representation change from Cartesian to Polar coordinates, in Fourier space, using $f_x=\rho\cos\psi$ and $f_y=\rho\sin\psi$:

$$\mathrm{PSD}_P(\rho,\psi)=\mathrm{PSD}_C(\rho\cos\psi,\rho\sin\psi). \quad (2)$$

Redefining the PSD in this way with $\rho\geq 0$, $\psi\in[0,2\pi)$, we can interpret $\mathrm{PSD}_P(\rho,\psi)$ as containing the power due to variations of absolute spatial frequency ρ in a direction given by ψ. A 1D signal will contain the same power at positive frequency ω as at the corresponding negative frequency $-\omega$, and similarly, a 2D image will have the same power along a certain direction ψ_0 with absolute frequency $|\rho|$ as along $-\psi_0$ with absolute frequency $|\rho|$. Hence, the 2D PSD has a rotational symmetry that is periodic with period π, i.e., $\mathrm{PSD}_P(\rho,\psi)=\mathrm{PSD}_P(\rho,\psi+\pi)$. In addition, we only consider the largest inscribed circle to balance the number of data points in each direction, and we exclude $\rho=0$, the zero-frequency term that reflects the overall background intensity, so we consider $0<\rho\leq\min(M,N)$, illustrated in Fig. 3.

Let us define two "1D PSD" functions that will allow us to obtain a better insight into the spatial nature of the speckle pattern. The radial PSD (rPSD), averaged over all angles ψ, for a certain spatial frequency ρ is given by:

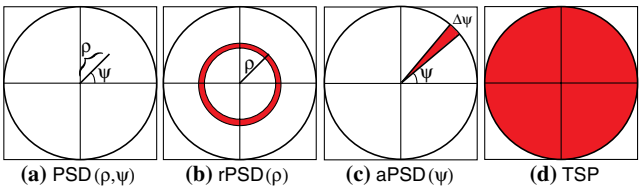

(a) PSD(ρ,ψ) **(b)** rPSD(ρ) **(c)** aPSD(ψ) **(d)** TSP

Fig. 3 Illustration of the various defined quantities. Note that the image portions are square, however, only values within the largest inscribed circle are used. (a) PSD in polar coordinates, Eq. (2). (b) rPSD, the PSD averaged over all angles for a fixed radius, Eq. (3). (c) aPSD, the PSD averaged over all radii for a small sector, Eq. (4). (d) TSP, the PSD summed over all angles and all radii, Eq. (5).

$$\mathrm{rPSD}(\rho)=\frac{1}{n}\sum_{\psi=0}^{2\pi}\mathrm{PSD}_P(\rho,\psi)\rho\Delta\psi, \quad (3)$$

where n is the number of data points in the summation and $\Delta\psi$ is the (angular) width of the summation interval. The rPSD gives the average power per spatial frequency ρ over all directions. Speckle grain size is inversely proportional to the spatial frequency, so the rPSD essentially gives the amount of power contained in speckles of various sizes across the entire image.

The other 1D function is the angular PSD (aPSD). The aPSD, which can be interpreted as containing information about directional variation of all spatial frequencies within a small angular interval $[\psi-\Delta\psi/2,\ \psi+\Delta\psi/2]$, can be given by an averaged sector integral:

$$\mathrm{aPSD}_{\Delta\psi}(\psi)=\frac{1}{n}\sum_{\psi'=\psi-\frac{\Delta\psi}{2}}^{\psi+\frac{\Delta\psi}{2}}\sum_{\rho=1}^{\min(M,N)}\mathrm{PSD}_P(\rho,\psi')\rho\Delta\rho\Delta\psi', \quad (4)$$

where similarly $\Delta\rho$ is the width of the summation interval in ρ. Note that Eq. (4) is formulated as a sector integral and not a simple line integral for dimensional consistency. The aPSD gives the angular speckle distribution, allowing us to find directions along which there are differences in the amount of speckle variation. A measure of anisotropy can be estimated by considering the standard deviation of the aPSD, normalized by the mean, i.e., $\sigma_{\mathrm{aPSD}}/\langle\mathrm{aPSD}\rangle$.

Lastly, we can get a sense of the total severity of the speckle distribution (a measure similar to the speckle contrast), by finding the total power across all frequencies and angles. This total spectral power (TSP) is the sum of Eq. (2) over all ρ and ψ:

$$\mathrm{TSP}=\sum_{\rho=1}^{\min(M,N)}\sum_{\psi=0}^{2\pi}\mathrm{PSD}_P(\rho,\psi)\rho\Delta\rho\Delta\psi. \quad (5)$$

A summary and illustration of the various defined quantities are given in Fig. 3.

4 Experiments and Results

To validate the method, we captured speckled images reconstructed using a holographic display system, shown in Fig. 4. A green 532 nm laser was expanded and collimated, and incident on a SXGA-R3-H1 (ForthDD) Ferroelectric Liquid Crystal (FLC) Spatial Light Modulator (SLM) connected to a

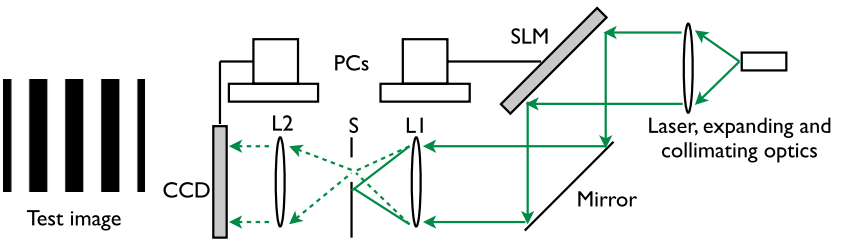

Fig. 4 Experimental setup. A 532 nm laser is expanded and incident on the Spatial Light Modulator (SLM), on which a hologram is launched. The modulated light passes through lenses L1 and L2, both of focal length 50 mm, and is imaged onto a CCD. S is a rectangular slit placed at the intermediate focal plane to block unwanted diffraction orders. The test image used is a simple step-function bar pattern with bars of equal width.

controlling computer. The SLM displays binary phase holograms at 24 bits at 60 Hz (for an effective 1440 binary frames per second). The reconstructed images were captured using a CCD camera (Retiga-4000R, and pixel size 7.4 μm). For our test image, we used a simple step-function bar pattern of equal width. We calculated phase-only Fourier holograms using a simplified GS algorithm.[19] We applied two software-based methods of speckle reduction, namely, (1) computing multiple random-phase holograms and displaying them sequentially within the CCD integration time, or Random-Phase Multiplexing (RPM), and (2) cyclically shifting the hologram in the SLM-plane,[12] similarly displaying the shifting holograms sequentially within the CCD integration time, or Cyclic Shift Multiplexing (CSM).* We chose to capture iterations of perfect square numbers (e.g., 9, 25, 100) because the speckle contrast decreases as the square root of the number of uncorrelated speckle patterns (i.e., the number of speckle reduction iterations).[2] From the captured reconstructed bar patterns, small square patches (of 51 pixel $\times$ 51 pixels) within the bars are isolated for analysis. Sample images are shown in Fig. 5. Note that the image portions shown are slightly larger than the patches used for analysis to include the adjacent bars for perspective. During our experiments, we find very large contributions in the PSD along the $\psi = 0$, $\pi/2$, π, $3\pi/2$ directions, likely due to the pixellated nature of the SLM, and we exclude these points from our analyses.

5 Speckle Analysis

5.1 *Speckle Severity*

First, we wish to show that the measure of speckle severity using the proposed PSD-based method, the TSP, gives the same information as the speckle contrast, (C). Figure 6 shows, on a log-log graph, C, and the TSP [Eq. (5)], plotted against total number of speckle reduction iterations. Here, we use only the RPM method. Best-fit curves are also overlaid. As mentioned previously, it is well known that C decreases as the square root of the number of speckle reduction iterations, and the slope of the fitted curve for C is -0.44, indeed close to -0.5. It underestimates the theory, likely due to residual speckle from the experimental setup (laser, optical elements, SLM) that is not reduced by the RPM method. The slope of the fit for the TSP is -0.95, close to -1. The linear correlation coefficient between C and the TSP is 0.99, showing near perfect correlation. Thus, there is good experimental support that the TSP is a sufficient measure of speckle severity.

5.2 *Speckle Granularity*

The rPSD represents the power present in variations of a certain fixed spatial frequency ρ. Spatial frequency is inversely proportional to length in real-space, and we can transform the dependent variable back into pixel-lengths to have a more physical picture. Five sample rPSD functions are plotted on a semilog scale against pixel-length in Fig. 7, for a single speckled image [Fig. 5(b)], one with 9 iterations of RPM reduction [Fig. 5(c)], one with 100 iterations of RPM reduction [Fig. 5(e)], one with 9 iterations of CSM reduction [Fig. 5(f)], and one with 100 iterations of CSM reduction [Fig. 5(h)]. The graphs represent the average power contained by variations of a particular length. Considering the single image and the two RPM-reduced images, we can see that the consistent shape of the graphs indicate that RPM decreases speckle of all lengths evenly. In contrast, notice that the CSM-reduced graphs have a different shape. The graphs suggest that CSM reduces the severity of small speckles as well as RPM, but at larger lengths, the effectiveness of the CSM rapidly decays, and it seems to have no effect beyond 8 pixels where the two CSM graphs converge. The CSM-reduced images retain intensity variations of about 8 pixels of larger, and we can visually perceive that as long-range correlations ("smears") in the images. Hence not only does the rPSD allow the characterization of speckle of every size in an image, it allows the evaluation of the effectiveness of speckle reduction methods in reducing speckle of every size.

5.3 *Speckle Anisotropy*

The aPSD gives the angular distribution of speckle power. Ideally, speckle should be spatially uncorrelated and isotropic. With reference to the sample images shown in Fig. 5, we can see that the RPM method, because it involves calculating different holograms and so generates uncorrelated speckle patterns, results in isotropic speckle reduction, while the CSM method, which relies on shifting a single hologram, seems to add some anisotropy to the image as a byproduct of speckle reduction, visually perceived as a "smearing" from the top-left to bottom-right of the image.

In Fig. 8, we plot on a polar plot, the aPSD against angle for a single speckled image [Fig. 5(b)], one with 100 iterations of RPM applied [Fig. 5(e)], and one with 100 iterations of CSM applied [Fig. 5(h)]. We exclude the contributions

*Shifting the hologram results in a shift of the reconstructed object in the image plane. For Fourier holograms, the image plane is at infinity, and so imaging the hologram via a lens should result in negligible movement of the object. Experimentally, however, we observe what seems to be small residual movement of the object, probably due to the discrete and pixellated nature of the SLM, resulting in anisotropic speckle reduction.

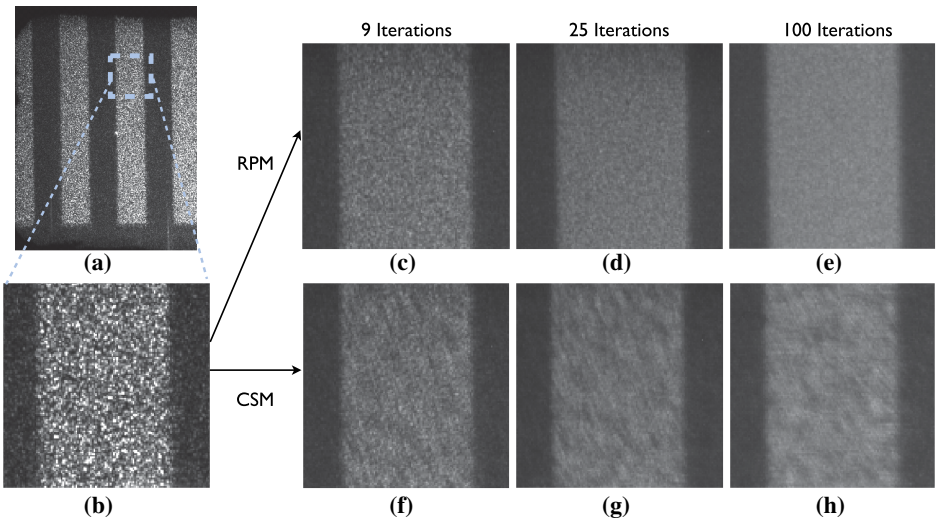

Fig. 5 Sample experimentally captured images. (a) Single speckled image, (b) Isolated image portion from (a). The speckles are clearly visible here. Top row: RPM speckle reduction applied with (c) 9 iterations, (d) 25 iterations and (e) 100 iterations. Bottom row: CSM speckle reduction applied with (f) 9, (g) 25 and (h) 100 iterations.

due to the pixellated nature of the SLM along the $\psi = 0$, $\pi/2$, π, $3\pi/2$ directions as mentioned in Sec. 4. Comparing the graphs in Fig. 8, ignoring the absolute magnitude of the values (which correspond more to severity), we can see that the single image and the image with 100 RPM iterations both have an isotropic distribution of power in all directions. However, the image with 100 CSM iterations has an aPSD with relatively more power in the first ($0 < \psi < \pi/2$) and third ($\pi < \psi < 3\pi/2$) quadrants. This corresponds to relatively more variation along the top-right to bottom-left direction, which can explain the smearing in the orthogonal, top-left to bottom-right direction. This orthogonal relation can be explained by considering the fact that a grating with vertical stripes (like our test image), when Fourier transformed, will have variation along the orthogonal, horizontal direction. The standard deviation of the aPSD (normalized by the mean of the aPSD) as described in Sec. 3, for these three images are, respectively, 0.09, 0.11 and 0.48. Thus the aPSD, and the normalized standard deviation of the aPSD, can sufficiently pick out anisotropy in the speckled images. As a final comment, the speckle contrast estimated from Fig. 5(b), 5(e) and 5(h) are 0.54, 0.07 and 0.11, respectively, and comparatively, the latter two images have almost the same speckle contrast. The aesthetic difference due to the anisotropy cannot be explained by the small difference in the latter two numbers.

5.4 *Discussion*

Here, we discuss the implementations and future research ideas. Although we show a proof of concept using a holographic display system, this method of speckle analysis is applicable to other laser-based display systems. The method

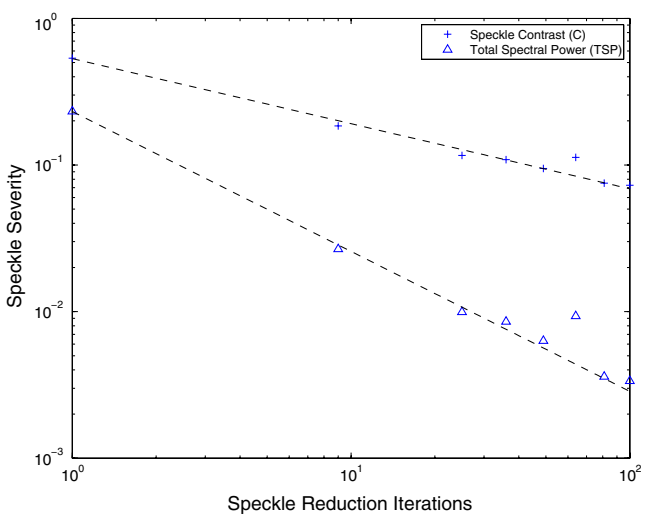

Fig. 6 The speckle contrast (C) and total spectral power (TSP) are plotted against the number of RPM reduction iterations on a log-log scale. The crosses and triangles denote C and TSP, respectively. The best-fit curves, plotted as dashed lines, have slopes close to −0.5 and −1, respectively.

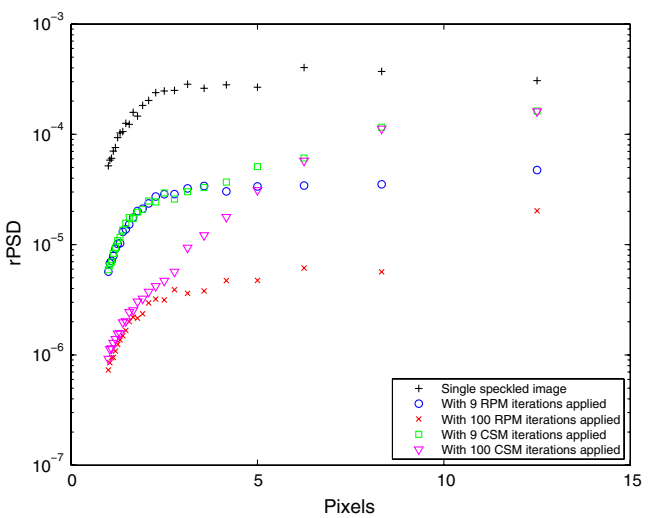

Fig. 7 The rPSD is plotted against pixel-lengths for five images, one with no speckle reduction applied [Fig. 5(b)], one with 9 iterations of RPM reduction [Fig. 5(c)], one with 100 iterations of RPM reduction [Fig. 5(e)], one with 9 iterations of CSM reduction [Fig. 5(f)], and one with 100 iterations of CSM reduction [Fig. 5(h)].

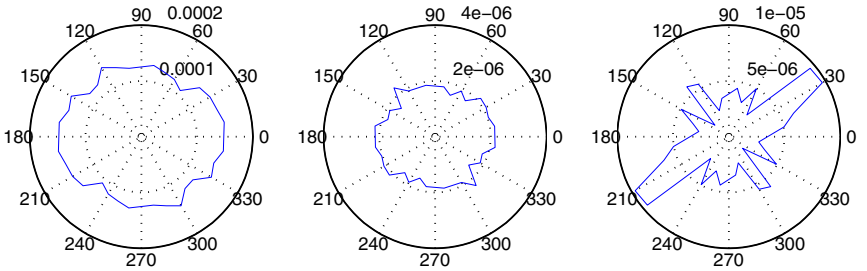

(a) Single **(b)** 100 RPM **(c)** 100 CSM

Fig. 8 Polar plots of the aPSD. (a) Single speckled image [Fig. 5(b)]. (b) Image with 100 RPM iterations applied [Fig. 5(e)]. (c) Image with 100 CSM iterations [Fig. 5(h)].

is simple enough to be embedded into a device, which can provide a convenient way of characterizing displays. In addition, it could possibly be integrated into a laser display system's speckle reduction module in a regulatory and feedback loop to ensure quality control.

Future experiments need to be done to relate the absolute quantities of the PSD function (which are in units of power per unit spatial frequency squared) to the observer's subjective judgments. As a parallel example, the human visual system's response to contrast and spatial frequency is given by the contrast sensitivity function, which is non-linear, and beyond certain combinations of contrast and spatial frequency, additional differences are indistinguishable to the human visual system. Similarly, additional experiments would have to be done to relate the physical quantities given by the PSD with the human threshold of perceiving differences in speckle severity, granularity and anisotropy. This is important to set standards by which to judge laser display systems and the various speckle reduction techniques they employ.

6 Conclusion

With the increasing ubiquity of laser-based displays, a more comprehensive metric is needed to quantify laser speckle noise for display purposes and address the limitations of the speckle contrast. In this paper we have made use of the power spectral density in polar-coordinates as a tool for speckle analysis. This representation allows the simultaneous measurement of three characteristics of speckle—severity, granularity, and anisotropy—allowing a more holistic characterization of speckle. The various quantities defined allows characterization of the distribution of speckle power at various grain sizes and along various directions, which is especially useful in speckle reduction as it can determine if speckles of all sizes and directions are being reduced equally. The work presented here will be useful in evaluating not only speckle in images, but current and future speckle reduction technologies as well.

Acknowledgments

This work is supported by the Singapore A*STAR Science and Engineering Research Council (SERC) HOME2015 Programme (Grant No. 0921150107). We would like to thank Yuechao Pan and Abel Lum for help with the experimental setup, Yvonne Yuan Gao for helpful discussions, and the editors and four anonymous referees for their comments on previous versions of the manuscript.

References

1. C. Dainty, Ed., *Laser Speckle and Related Phenomena*, Springer-Verlag, Berlin, New York (1984).
2. J. W. Goodman, *Speckle Phenomena in Optics: Theory and Applications*, Roberts & Co. Publishers, Englewood, Colorado (2009).
3. P. Šmid, P. Horváth, and M. Hrabovský, "Speckle correlation method used to measure object's in-plane velocity," *Appl. Opt.* **46**(18), 3709–3715 (2007).
4. H. J. Rabal and R. A. Braga, Ed., *Dynamic Laser Speckle and Applications*, CRC Press, Boca Raton, FL (2008).
5. M. Takeda and H. Yamamoto, "Fourier-transform speckle profilometry: three-dimensional shape measurements of diffuse objects with large height steps and/or spatially isolated surfaces," *Appl. Opt.* **33**(34), 7829–7837 (1994).
6. O. V. Michailovich and A. Tannenbaum, "Despeckling of medical ultrasound images," *IEEE Trans. Ultrason. Ferroelectrics Freq. Contr.* **53**(1), 64–78 (2006).
7. M. Okuda et al., "High efficiency optical system for ultra-short throw distance projector based on multi-laser light source," *J. SID* **19**(2), 221–229 (2011).
8. J. I. Trisnadi, "Speckle contrast reduction in laser projection displays," *Proc. SPIE* **4657**, 131–137 (2002).
9. E. Buckley, "Holographic laser projection technology," in *Proc. SID Symposium 2008*, Vol. **70.2**, 1074–1079 (2008).
10. X. W. Xu et al., "Full high-definition digital 3D holographic display and its enabling technologies," *Proc. SPIE* **7730**, 77301C (2010).
11. T. Iwai and T. Asakura, "Speckle reduction in coherent information processing," *Proc. IEEE* **84**, 765–781 (1996).
12. L. Golan and S. Shoham, "Speckle elimination using shift-averaging in high-rate holographic projection," *Opt. Express* **17**(3), 1330–1339 (2009).
13. S. E. Skipetrov et al., "Noise in laser speckle correlation and imaging techniques," *Opt. Express* **18**(14),14519–14534 (2010).
14. L. I. Goldfischer, "Autocorrelation function and power spectral density of laser-produced speckle patterns," *J. Opt. Soc. Am.* **55**(3), 247–253 (1965).
15. F. Sarto et al., "Electrode surface morphology characterization by atomic force microscopy," in *Proc. ICCF-14 International Conf. on Condensed Matter Nuclear Science*, Washington, DC, Vol. **2**, 437–443 (2008).
16. W. A. Gardner, *Statistical Spectral Analysis: A Nonprobablistic Theory*, Prentice Hall, Englewoods Cliffs, NJ (1988).
17. J. S. Bendat and A. G. Piersol, *Engineering Applications of Correlation and Spectral Analysis*, 2nd ed., John Wiley & Sons, New York (1993).
18. F. Castanié, Ed., *Spectral Analysis: Parametric and Non-Parametric Digital Methods*, ISTE Ltd., Newport Beach, CA (2006).
19. R. W. Gerchberg and W. O. Saxton, "A practical algorithm for the determination of phase from image and diffraction plane pictures," *Optik (Jena)* **35**(2), 237–246 (1972).

Desmond C. Ong graduated with a BA in physics, *magna cum laude*, and economics, *summa cum laude*, from Cornell University, on a National Science Scholarship from A*STAR, Singapore. He is currently a research engineer at the Data Storage Institute, A*STAR. His diverse research interests include, but are not limited to, display holography, human visual cognition, behavioral economics, and social cognition.

Sanjeev Solanki received his MSc degree from the Indian Institute of Technology, New Delhi, and his PhD degree in electrical and computer engineering from the National University of Singapore. His research focus includes optical and electroholography for application to high-density optical data storage and holographic TV.

Xinan Liang is a scientist in optical materials and systems division at Data Storage Institute (DSI), ASTAR, Singapore. He received his BSc degree in 1992 from Lanzhou University, his MSc degree in 1997 from the Chinese Academy of Space Technology (CAST), and his PhD degree in 2000 from the Chinese Academy of Sciences (CAS). His current research interest includes holographic recording media and holographic 3D display technology.

Xuewu Xu obtained his BSc degree from Nanjing University and his PhD degree from the Chinese Academy of Sciences (CAS). He is a scientist of Data Storage Institute. His research interests include holography for 3D display and high density data storage, holographic media, and crystal materials. He is a member of The Society for Information Display (SID) and a member of International Organizing Committee of International Workshop on Holography and related technologies (IWH).